Optical and Quantum Electronics 9 (1977) 61–74

Pulse dispersion in partially-excited graded-index fibres

R. SAMMUT
Department of Electronics, University of Southampton, Southampton SO9 5NH, UK

Received 24 August 1976

Simple analytical results are obtained for the mode distribution and impulse response of graded index fibres under a variety of excitation conditions relevant to practical systems. It is found that the choice of an optimum refractive index profile depends quite strongly on the source distribution of or, that one can significantly improve the impulse response of a particular profile by appropriate choice of launching conditions. Furthermore the r.m.s. pulse width is not necessarily reduced simply by partially filling the numerical aperture of the fibre.

1. Introduction

Now that fibre attenuation is no longer the major obstacle to the use of optical fibres in communication systems, and methods are available for manufacturing (more-or-less reproducibly) fibres of any desired refractive index profile [1, 2], much attention is being given to the choice of profile which will maximize the bandwidth, or information-carrying capacity, of the fibre.

Increasingly sophisticated analyses have been presented which take account of mode coupling [3], material [4–6], profile [6] and non-linear [7] dispersion and low-frequency perturbations in the refractive index profile [8]. However, it is generally assumed in these analyses that all modes of the fibre are equally excited. Very little theoretical attention has been given to the fact that a fibre's response may be substantially altered by the use of sources which excite modes selectively, despite the fact that a variety of source configurations are being used experimentally to investigate fibre behaviour e.g. [9, 10].

The aim of the present paper is to examine the mode distribution and pulse dispersion of a graded index fibre (with α-law profile) under a variety of excitation conditions relevant to practical systems where simple analytical expressions can be obtained. As the main interest lies in the effect of selective mode excitation (and in avoiding lengthy numerical calculations), dispersion and mode-coupling effects are not considered at this stage.

As a result of this analysis we find, for example, that (i) focussing an incoherent source does not improve the pulse dispersion of the system, (ii) for profiles with $\alpha \lesssim 2 - \Delta$, a Lambertian source gives a smaller r.m.s. pulse width than an unfocussed laser (plane wave) source and (iii) given a particular α-profile and launching efficiency requirement, one can, by varying the beam waist or launching position of a focussed (Gaussian) spot, obtain very much smaller r.m.s. pulse widths than are achieved using unfocussed or Lambertian sources.

The approach here is based on the WKB approximation. It follows, with one important modification, an idea which was originally presented by Timmermann [11] and which has been shown to give good agreement with experimental results in the particular case of a fibre with quartic refractive index profile excited by an LED [12] (although it must be noted that an adjustable parameter is involved in obtaining this agreement).

Experimental results have also been published for the pulse dispersion of a graded index fibre excited by obliquely incident plane waves [13, 14] and a theoretical treatment of this situation for the parabolic index fibre has appeared [15]. However, we believe the latter to be in error, for reasons discussed in Section 3.2.

The paper is organized as follows. In Section 2 the impulse response of a general graded index fibre is calculated using a method which basically involves the conversion of an angular source distribution into a distribution in terms of fibre-mode parameters followed by a summation over all bound modes. (The effect of leaky modes can be included – but not analytically).

These results are used in Section 3 to derive analytical expressions for the impulse response of fibres with α-law refractive index profiles [16] excited by LED and laser sources, focussed or unfocussed. In each case, the variation of the mode spectrum and pulse width with changes in the source distribution is investigated. The results are discussed in Section 4.

2. Impulse response–formalism

We consider a fibre with core radius a and refractive index profile

$$n^2(x) = n_0^2 g(x), \tag{1}$$

where $x = r/a$ is the normalized radius.

The usual mode parameters β and ν can be written as

$$\beta = k_0 g_0^{1/2} \cos\gamma_0 \tag{2}$$

and

$$\nu = \nu' \cos\phi \sin\gamma_0 \tag{3}$$

where

$$k_0 = \frac{2\pi n_0}{\lambda}, \tag{4}$$

$$\nu' = a k_0 x_0 g_0^{1/2}, \tag{5}$$

$$g_0 = g(x_0), \tag{6}$$

x_0 gives the radial position of the source point, γ_0 is the angle to the fibre-axis and ϕ is the projected angle of incidence of the ray.* λ is the free-space wavelength. We also define a normalized phase constant

$$\beta_n = \beta/k. \tag{7}$$

Assuming for simplicity a monochromatic (or in the case of incoherent sources, quasi-monochromatic) source, the power $I_\Omega \, d\Omega \, dA$ radiated from an infinitesimal area dA within a solid angle $d\Omega$ can be expressed as

$$\begin{aligned} I_\Omega \, d\Omega dA &= I_\Omega [\gamma_0(\beta_n, \nu), \phi(\beta_n, \nu), x_0, \theta_0] |D| \, d\nu \, d\beta_n \, dA \\ &\equiv I_M \, d\nu \, d\beta_n \, dA \end{aligned} \tag{8}$$

where

$$dA = a^2 x_0 \, dx_0 \, d\theta_0, \tag{9}$$

$$|D| = \{\nu'[g_0 - \beta_n^2 - g_0(\nu/\nu')^2]^{1/2}\}^{-1}, \tag{10}$$

and I_M gives the mode spectrum.

For a unit input pulse $s_1(t)$, the output pulse $P(t)$, can then be calculated from

$$\begin{aligned} P(t) &= s_2(t) \quad t_1 \leqslant t \leqslant t_2 \\ &= 0 \qquad \text{otherwise} \end{aligned} \tag{11}$$

where

$$s_2(t) = \frac{1}{N} \iiint s_1(t - \tau_g) I_M \, d\nu \, d\beta_n \, dA. \tag{12}$$

τ_g is the modal group velocity (a function of the profile) and N is a normalizing factor defined by

$$\int_0^\infty s_2(t) \, dt = 1, \tag{13}$$

*See Fig. 1 of [17]; but note that throughout the present paper, all angles are measured *within* the fibre.

where the integration is extended over the whole of the output distribution, including that part which lies outside the numerical aperture of the fibre. The times t_1 and t_2 which specify the bound part of the output pulse are determined by the allowed range of β_n values (see Section 3).

Equation 12 can now be simplified using the following assumptions: (i) I_Ω does not depend explicitly on ϕ and (ii) τ_g is a function of β_n and a/λ only. For bound modes, the ν-integration can then be performed between the limits*

$$\nu_{min} = 0 \quad \text{and} \quad \nu_{max} = \nu'(1-\beta_n^2/g_0)^{1/2} \tag{14}$$

to give

$$s_2(t) = \frac{\pi}{2N}\iiint s_1(t-\tau_g)\, I_\Omega\, g_0^{-1/2}\, dA \tag{15}$$

This is the point at which we depart from Timmermann's work [11]. He gives a ν_{max} which is evaluated from the WKB eigenvalue equation for the particular profile under consideration and hence independent of x_0 whereas, according to Equation 14, we integrate between the zeros of D^{-1} and thus take account of the fact that the range of modes launched will depend on the location of the source.

In the case where s_1 is a delta function, we obtain the impulse response by using assumption (ii) to replace the integration over β_n by an integration over τ_g and find

$$s_2(t) = \frac{\pi}{2N}\left|\frac{\partial\beta_n}{\partial\tau_g}\right|_{\tau_g=t}\iint I_\Omega\, g_0^{-1/2}\, d\beta_n\, dA. \tag{16}$$

Now given $s_2(t)$ and hence $P(t)$, the r.m.s. pulse width, σ, can be determined. This is the quantity of major interest as it determines the bandwidth in a multimode fibre [18] and is given by [6]

$$\sigma^2 = M_2/M_0 - (M_1/M_0)^2 \tag{17}$$

where

$$M_n = \int_0^\infty P(t)t^n\, dt, \quad n = 0, 1, 2. \tag{18}$$

We can now apply these results to a number of specific cases.

3. Impulse response of α-law fibres

We consider the profile defined by

$$\begin{aligned} g(x) &= 1-2\Delta x^\alpha \quad x \leqslant 1 \\ &\quad 1-2\Delta \quad\quad x > 1. \end{aligned} \tag{19}$$

Previous analyses of such fibres have been restricted to Lambertian sources or, in the special case $\alpha = 2$, to plane wave excitation.

In order to apply our formalism here, we must first evaluate $\partial\beta_n/\partial\tau_g$. It is shown in the Appendix that

$$\frac{\tau_g}{\tau_0} = \frac{\alpha+2\beta_n^2}{(\alpha+2)\beta_n} \tag{20}$$

so that

$$\frac{\partial\beta_n}{\partial\tau_g} = \frac{(\alpha+2)\beta_n^2}{\tau_0(\alpha-2\beta_n^2)} \tag{21}$$

and Equation 16 becomes

$$s_2(t) = \frac{\pi(\alpha+2)\beta_n^2}{2N\tau_0|\alpha-2\beta_n^2|}\iint I_\Omega\, g_0^{-1/2}\, dA. \tag{22}$$

where the range of integration over x_0 depends on the source but is restricted by the requirement to include only bound modes to lie between

$$x_0 = 0 \quad \text{and} \quad x_0 = [(1-\beta_n^2)/2\Delta]^{1/\alpha}. \tag{23}$$

*If tunnelling leaky modes are to be included, the limits on ν must be adjusted.

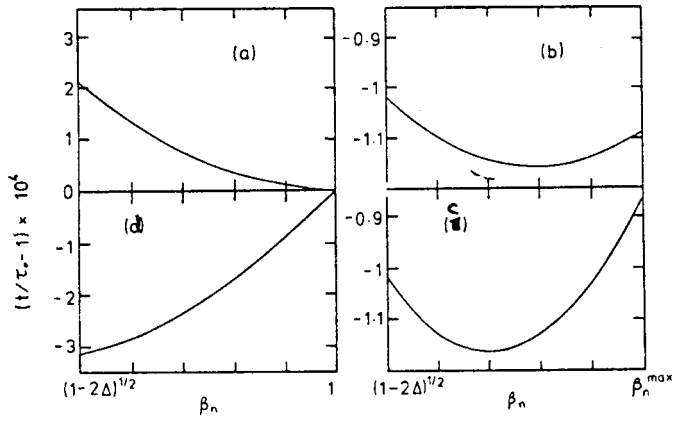

Figure 1 Examples of the τ_g–β_n relationship for $\Delta = 0.02$, $\gamma_1 = 0$, $\gamma_2 = 90°$ and (a) $\alpha = 2$, $x_1 = 0$, $x_2 = 1$; (b) $\alpha = 1.94$, $x_1 = 0.75$, $x_2 = 1$; (c) $\alpha = 1.94$, $x_1 = 0.6$, $x_2 = 1$ and (d) $\alpha = 1.90$, $x_1 = 0$, $x_2 = 1$.

In Equation 22, all quantities on the right hand side are evaluated at $\tau_g = t$ and, for α in the range $2(1-2\Delta) < \alpha < 2$, Equation 20 shows that two distinct values of β_n may contribute to the output at a given time. To calculate the times t_1 and t_2 which bound the output pulse we must take account of Δ, α and the extent and angular spread of the source. If the source lies between the normalized radii x_1 and x_2 ($>x_1$) and it emits rays with angles to the z-axis between γ_1 and γ_2 ($>\gamma_1$) then, for bound modes, β_n lies between

$$\beta_n^{min} = \max\left[(1-2\Delta)^{1/2}, (1-2\Delta x_2^{\alpha})^{1/2}\cos\gamma_2\right] \tag{24}$$

and

$$\beta_n^{max} = (1-2\Delta x_1^{\alpha})^{1/2}\cos\gamma_1. \tag{25}$$

These boundaries determine the absolute pulse width through Equation 20:

If $\alpha \geqslant 2$, τ_g decreases monotonically as β_n increases so that

$$t_1 = \tau_g(\beta_n^{max}) \geqslant \tau_0 \tag{26}$$

and

$$t_2 = \tau_g(\beta_n^{min}).$$

If $2(1-2\Delta) \leqslant \alpha < 2$, the $\tau_g - \beta_n$ curve passes through a minimum at $\beta_n = (\alpha/2)^{1/2}$ so that there are two possible situations, depending on the source. If β_n does not reach this turning point, then Equation 26 applies, but otherwise

$$t_1 = \frac{(8\alpha)^{1/2}}{\alpha+2} \tag{27}$$

and

$$t_2 = \max\left[\tau_g(\beta_n^{min}), \tau_g(\beta_n^{max})\right].$$

Finally, if $\alpha \leqslant 2(1-2\Delta)$, τ_g increases monotonically with β_n so that

$$t_1 = \tau_g(\beta_n^{min}) \tag{28}$$

$$t_2 = \tau_g(\beta_n^{max}) \leqslant \tau_0.$$

These various situations are illustrated in Fig. 1.

3.1 LED sources

As a first example, we consider an LED butted against the fibre aperture and approximate its intensity distribution with that of a Lambertian source. That is, we put

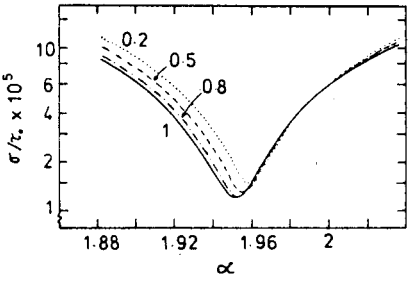

Figure 2 R.M.S. pulse width, σ, as a function of α for focussed and unfocussed LED (Lambertian) sources. $\Delta = 0.02$. The value of γ_s/γ_c is given on each curve.

$$I_\Omega = \frac{\cos\gamma_0}{\pi^2 a^2} = \frac{1}{\pi^2 a^2}\beta_n g_0^{-1/2}. \tag{29}$$

Substituting in Equation 22 and normalizing, we find the output pulse

$$s_2(t) = \frac{2(\alpha+2)\beta_n^3}{\tau_0\alpha|\alpha-2\beta_n^2|}\frac{\sum_{i=0}^{\infty}[(1-\beta_n^2)^{i+(2/\alpha)}/(\alpha i+2)]}{\sum_{i=0}^{\infty}[1/(\alpha i+2)/(\alpha(i+1)+2)]}. \tag{30}$$

Apart from a normalization factor, the first term of Equation 30 (i.e. $i = 0$ in both numerator and denominator) gives the result previously found by Arnaud [4] while the remaining terms give extremely small corrections, since for a weakly guiding fibre, $1 - \beta_n^2 \ll 1$. Equation 30 can also be reduced to the small-Δ approximation of Gloge and Marcatili [16]. When $\alpha \to \infty$ (step index fibre), Equation 30 also reduces to the form given by Dakin *et al.* [19].

If light from the LED is focussed by passing through a lens before entering the fibre, all rays will have an angle of incidence, γ_0, smaller than some angle, γ_s. Assuming the cosine intensity distribution is approximately unchanged by the passage through the lens, we model this situation with a Lambertian source which is simply truncated at γ_s.

A little care is needed in this case if γ_s is smaller than the numerical aperture of the fibre. The smallest value β_n can take for a ray launched from x_0 is $(1 - 2\Delta x_0^\alpha)^{1/2}\cos\gamma_s$ so that if $\beta_n < \cos\gamma_s$, x_0 must have some minimum value greater than zero. When β_n is in this range, the lower limit in Equation 23 must be altered to

$$x_0 = \left[\frac{1}{2\Delta}\left(1 - \frac{\beta_n^2}{\cos^2\gamma_s}\right)\right]^{1/\alpha}.$$

Using this lower limit in Equation 22 and retaining only the first term of an expression similar to Equation 30, we find the output pulse

$$\begin{aligned} s_2(t) &= \frac{(\alpha+2)\beta_n^3}{\tau_0|\alpha-2\beta_n^2|N}[(1-\beta_n^2)^{2/\alpha} - (1-\beta_n^2/\cos^2\gamma_s)^{2/\alpha}] \qquad \beta_n \leqslant \cos\gamma_s \\ &= \frac{(\alpha+2)\beta_n^3}{\tau_0|\alpha-2\beta_n^2|N}(1-\beta_n^2)^{2/\alpha} \qquad \beta_n > \cos\gamma_s \end{aligned} \tag{31}$$

where

$$N = \frac{\alpha}{2(\alpha+2)}\{[1-\cos^2\gamma_s(1-2\Delta)]^{(2/\alpha)+1} - \cos^2\gamma_s(2\Delta)^{(2/\alpha)+1}\}.$$

Using Equations 17, 18, 30 and 31 we can now calculate the r.m.s. pulse widths resulting from these Lambertian sources. Fig. 2 shows σ as a function of α for various values of γ_s/γ_c (where $\gamma_c \simeq (2\Delta)^{1/2}$ is the numerical aperture of the fibre). As expected from the approximate analysis of Gloge and Marcatili [16], the pulse widths are smallest in the neighbourhood of $\alpha = 2 - 2\Delta$. But we also have the surprising

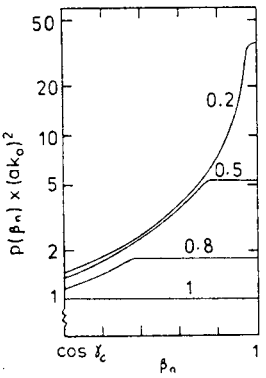

Figure 3 Distribution of average power per mode as a function of β_n on a parabolic index fibre excited by focussed and unfocussed Lambertian sources. The value of γ_s/γ_c is given on each curve.

result that, while truncating the source makes very little difference to the r.m.s. pulse width, it actually worsens it slightly for $\alpha < 2 - 2\Delta$ [20].

We can also use Equations 30 and 31 to obtain some information about the distribution of power amongst the modes of the fibre. The number of modes with propagation constants in the range $(\beta_n, \beta_n + d\beta_n)$ is given by [16]

$$\partial m = (ak_0)^2 \beta_n \left(\frac{1-\beta_n^2}{2\Delta}\right)^{2/\alpha} \partial\beta_n \tag{32}$$

so the *average* power per mode in the interval $(\beta_n, \beta_n + d\beta_n)$, $p(\beta_n)$, can be calculated from

$$p(\beta_n) = s_2(t) \frac{\partial t}{\partial \beta_n} \frac{\partial \beta_n}{\partial m}. \tag{33}$$

In Fig. 3, this quantity is plotted against β_n for various values of γ_s/γ_c. The horizontal line corresponds to the full Lambertian source and is in agreement with the 'equal excitation principle' [21, 22] – but note that we have already summed over ν so this gives no information about the actual power in individual modes.

3.2 Unfocussed laser (plane wave) excitation

As we noted in Section 1, Jacomme [15] has calculated the impulse response of a parabolic index fibre excited by a plane wave incident at various angles to the fibre axis using ray-tracing techniques. However, there is a marked disagreement between these results and our own.

Because of assumption (i) in Section 2, Equation 22 can only be used for excitation by a plane wave

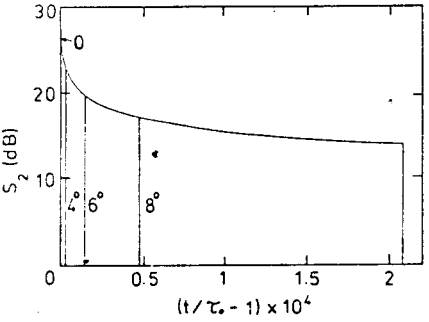

Figure 4 Impulse response of a parabolic index fibre excited by a plane wave incident at various angles to the fibre axis.

parallel to the fibre axis so we shall look at this result first. (In the off-axis case, the ν-integration in Equation 12 must be performed in a different way.)

The angular intensity distribution is written as

$$I_\Omega = \frac{1}{2\pi^2 a^2}\frac{\delta(\gamma_0)}{\sin\gamma_0}$$

$$= \frac{\beta_n}{2\pi^2 a^2}\delta(g_0^{1/2} - \beta_n) \tag{34}$$

so that substituting in Equation 22 gives

$$s_2(t) = \frac{(\alpha+2)\beta_n^3}{2\tau_0 N|\alpha - 2\beta_n^2|}\int_0^{x_{max}} g_0^{-1/2}\delta(g_0^{1/2} - \beta_n)x_0\,dx_0$$

where x_{max} is given by Equation 23.

Integrating this equation we find

$$s_2(t) = \frac{4(\alpha+2)\beta_n^3}{(2\Delta)^{(2/\alpha)}\alpha\tau_0|\alpha - 2\beta_n^2|}(1-\beta_n^2)^{(2/\alpha)-1} \tag{35}$$

which reduces, in the special case of $\alpha = 2$, to

$$s_2(t) = \frac{2\beta_n^3}{\Delta\tau_0(1-\beta_n^2)}. \tag{36}$$

Equation 36 exhibits qualitatively different behaviour from Jacomme's numerical results (see Fig. 4). Fortunately this system is sufficiently simple so that it can be analysed without the use of either ray-tracing or the present theory and it is found that Equation 35 is confirmed when proper account is taken of the distribution of mode transit times.

The power traversing an annulus of radius ax_0 and thickness $a\,dx_0$ due to a uniform plane wave incident at angle θ to the fibre axis is proportional to $x_0\,dx_0$. Now, from Equations 2 and 7, with $\gamma_0 = \theta$, we find for the α-profile that

$$\beta_n^2 = (1 - 2\Delta x_0^\alpha)\cos^2\theta \tag{37}$$

so the element of area $x_0\,dx_0$ is associated with an area in β_n space given by

$$x_0\,dx_0 = \frac{-1}{\alpha\Delta}\left[\frac{1}{2\Delta}\left(1 - \frac{\beta_n^2}{\cos^2\theta}\right)\right]^{2/\alpha-1}\frac{\beta_n\,d\beta_n}{\cos^2\theta}. \tag{38}$$

But from Equation 20

$$\beta_n\,d\beta_n = \frac{-(\alpha+2)\beta_n^3}{\tau_0(\alpha - 2\beta_n^2)}\,dt \tag{39}$$

so that combination of Equations 38 and 39 gives the power density as

$$x_0\,dx_0 = \frac{(\alpha+2)\beta_n^3}{\alpha\Delta\tau_0|\alpha - 2\beta_n^2|}\left[\frac{1}{2\Delta}\left(1 - \frac{\beta_n^2}{\cos^2\theta}\right)\right]^{(2/\alpha)-1}\frac{dt}{\cos^2\theta}. \tag{40}$$

In the case $\theta = 0$, Equation 40 confirms Equation 35 and for $\theta \neq 0$, normalizing Equation 40 gives the result for an off-axis plane wave,

$$s_2(t) = \frac{4(\alpha+2)\beta_n^3}{\alpha\tau_0(2\Delta)^{(2/\alpha)}\cos^2\theta}\frac{(1-\beta_n^2/\cos^2\theta)^{(2/\alpha)-1}}{|\alpha - 2\beta_n^2|}. \tag{41}$$

The r.m.s. width of this pulse is shown as a function of α in Fig. 5, for various angles of incidence θ. The calculations apply to a fibre with $\Delta = 0.02$ so that the critical angle is $\gamma_c \simeq 11.54°$. Once again, we note that although the Lambertian source produces the pulse with the largest absolute pulse width, the

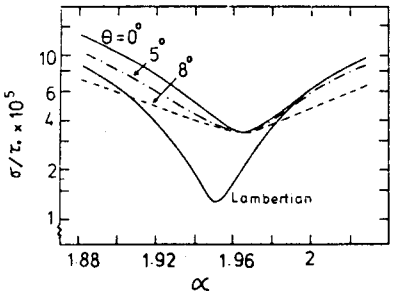

Figure 5 R.M.S. pulse width as a function of α for a fibre excited by plane waves at various angles of incidence, θ. $\Delta = 0.02$ so that the critical angle (inside the fibre) is 11.54°. The Lambertian result is also included for comparison.

minimum r.m.s. pulse width in the Lambertian case is considerably lower than that obtained using plane wave sources.

In Fig. 6, the r.m.s. pulse width is shown as a function of angle of incidence for the particular case of the parabolic index fibre. A great improvement in pulse dispersion can clearly be obtained by launching off-axis but this must be balanced against the decrease in launching efficiency shown in Fig. 7 for the same fibre. Given a minimum acceptable launching efficiency, one can choose the most appropriate launching angle using these curves (and similar results for other values of α).

Apart from the pulse width, the other quantity which has been experimentally measured is the mean delay difference

$$\Delta_\tau = \frac{M_1(\theta)}{M_0(\theta)} - \frac{M_1(0)}{M_0(0)} \tag{42}$$

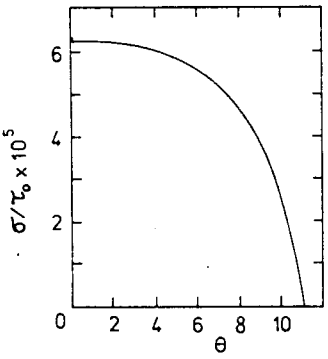

Figure 6 R.M.S. pulse width as a function of angle of incidence for a parabolic index fibre excited by a plane wave. Note that as in Fig. 6, angles are measured within the fibre. $\Delta = 0.02$.

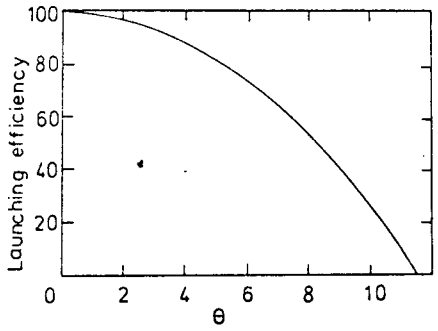

Figure 7 Launching efficiency as a function of angle for the fibre described in Fig. 6.

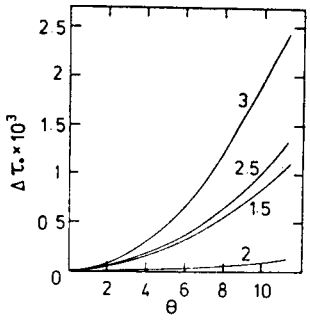

Figure 8 Mean delay difference between pulses launched by plane waves incident at angle θ for various values of α. For $\alpha = 1.5$, the absolute value is shown as the delay decreases with increasing angle. $\Delta = 0.02$.

between pulses launched at different angles (M_1 and M_0 are given by Equation 18). This quantity is plotted in Fig. 8 as a function of θ for various values of α. When $\alpha = 6$ and $\Delta \simeq 0.006$ our results agree with the theoretical curve given by Keck [13] but it is difficult to compare these with experiment as the fibre involved is only approximately an α-profile and a number of other uncertainties introduced by the experimental system must be considered [13].

Finally, looking as we did in Fig. 3 at the average power per mode as a function of β_n, Fig. 9 shows $p(\beta_n)$ (calculated from Equation 33) plotted against $\beta_n/\cos\theta$ for various values of θ.

3.3 Excitation by a focussed spot

We consider now the excitation of an α-profile fibre by a tightly focussed laser beam moving across the fibre face. This is a particularly useful example because it enables us to examine separately the influence of the index profile, the position of the source and its angular spread on the output pulse.

Assuming that the spot size is much smaller than the fibre diameter the focussed spot is described by a Gaussian distribution of the form [19]

$$I_\Omega = \frac{1}{\pi^2 a^2}\left(\frac{\pi w_0}{\lambda}\right)^2 \sec^3\gamma_0 \exp\left[-2\left(\frac{\pi w_0}{\lambda}\tan\gamma_0\right)^2\right]\frac{\delta(x_0 - s)}{x_0}$$

$$= \frac{1}{\pi^2 a^2}\left(\frac{\pi w_0}{\lambda}\right)^2\left(\frac{g_0}{\beta_n^2}\right)^{3/2} \exp\left[-2\left(\frac{\pi w_0}{\lambda}\right)^2\left(\frac{g_0}{\beta_n^2} - 1\right)\right]\frac{\delta(x_0 - s)}{x_0} \qquad (43)$$

where as is the distance between the spot and the fibre axis and w_0 is the 'spot size' corresponding to an angular beam spread $2\tan^{-1}(\lambda/\pi w_0)$.

The resulting normalized output pulse is given by

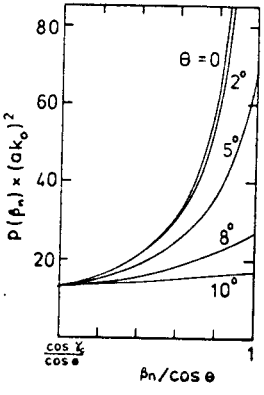

Figure 9 Distribution of average power per mode as a function of $\beta_n/\cos\theta$ on a parabolic index fibre excited by plane waves incident at various angles θ.

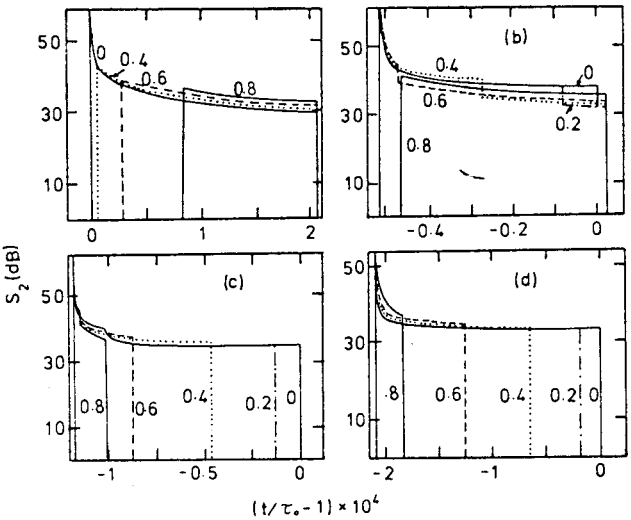

Figure 10 Impulse responses of fibres of various profiles excited by a Gaussian beam of angular spread 30° moving across the fibre face. The normalized radius of the launching point is indicated on the curve. $\Delta = 0.02$ and (a) $\alpha = 2$; (b) $\alpha = 1.96$; (c) $\alpha = 1.94$; (d) $\alpha = 1.92$.

$$s_2(t) = \frac{4(\alpha+2)}{\tau_0}\left(\frac{\pi w_0}{\lambda}\right)^2 \frac{g_0}{\beta_n} \frac{\exp\left[-2(\pi w_0/\lambda)^2(g_0/\beta_n^2 - 1)\right]}{|\alpha - 2\beta_n^2|} \tag{44}$$

where g_0 is calculated at $x_0 = s$ and the absolute pulse width is given by Equations 26–28. In the limit $\alpha \to \infty$ (step index fibre), this result agrees with that previously derived by Dakin *et al.* [19]. Figs. 10a–d show the impulse responses of fibres of various profiles excited by a Gaussian beam with an angular spread of 30° moving across the fibre face. This value of angular spread has been chosen so that the angle at which the intensity falls to e^{-2} times its peak value exceeds the local numerical aperture at all points on the fibre face. There are several points of interest in these curves:

(a) If $2(1 - 2\Delta) \leqslant \alpha \leqslant 2$ and $s \leqslant [(1/2\Delta)(1 - \alpha/2)]^{1/\alpha}$, the impulse response is infinite at the lower time limit (where $\beta_n^2 = \alpha/2$). In the parabolic case, only the on-axis beam gives an infinite response.

(b) The discontinuities in Figs. 10b and c occur because at the leading edge (shorter time), contributions from two values of β_n must be added but, as we approach the trailing edge, one of these β_n values falls outside the allowed range. In the case where $\alpha = 1.94$, the outermost launch point corresponds to a pulse whose trailing edge is defined by the smallest allowed β_n value (i.e. 'cutoff'), while the remaining four curves have their upper limit determined by the largest allowed β_n value, and the discontinuity by the cutoff value. Thus, if leaky modes were included in this figure, the effect on the first-mentioned curve would be to add a slow 'tail' but to leave the discontinuity unaffected while the remaining curves would have the discontinuity smoothed. When $\alpha = 1.96$, introducing leaky modes would add a slow tail in all cases.

(c) The variations in absolute width with α and s can be determined from Equations 26–28.

Figs. 11a–d show the effect on the impulse response of one particular profile ($\alpha = 1.96$) when the launching beam width is increased from 10° to 40°. The behaviour of these curves can be most easily understood if they are considered in conjunction with Figs. 12a–d which show the average power per mode plotted against β_n on this fibre. The latter show that for a near-parallel beam, the majority of the power is confined to modes within a small range of β_n values (which decrease as the source moves

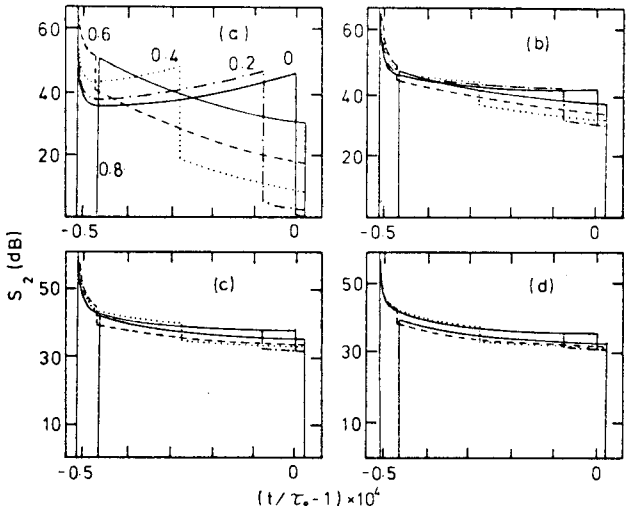

Figure 11 Impulse response of a fibre with $\alpha = 1.96$ excited by Gaussian beams of increasing angular spread moving across the fibre face. As in Fig. 10, the launching radius is indicated on each curve and $\Delta = 0.02$. $\gamma_G = 2\tan^{-1}(\lambda/\pi w_0)$ is (a) 10° (b) 20° (c) 30° (d) 40°.

towards the periphery) but as the beam becomes more divergent, the power becomes more equally distributed in β_n. For the least divergent beam, Fig. 11a, most power is launched into modes with large β_n and very little into small β_n modes. Curves corresponding to all but the outermost launch point therefore have, apart from the infinity at $\beta_n^2 = \alpha/2$, a secondary peak at times corresponding to the largest allowed β_n value, and then a discontinuous drop to the contribution made by the smaller β_n modes

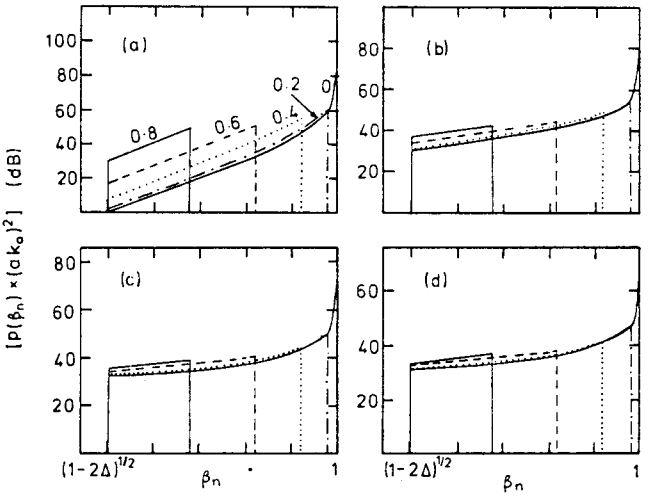

Figure 12 Average power per mode plotted against β_n for the situation illustrated in Fig. 11.

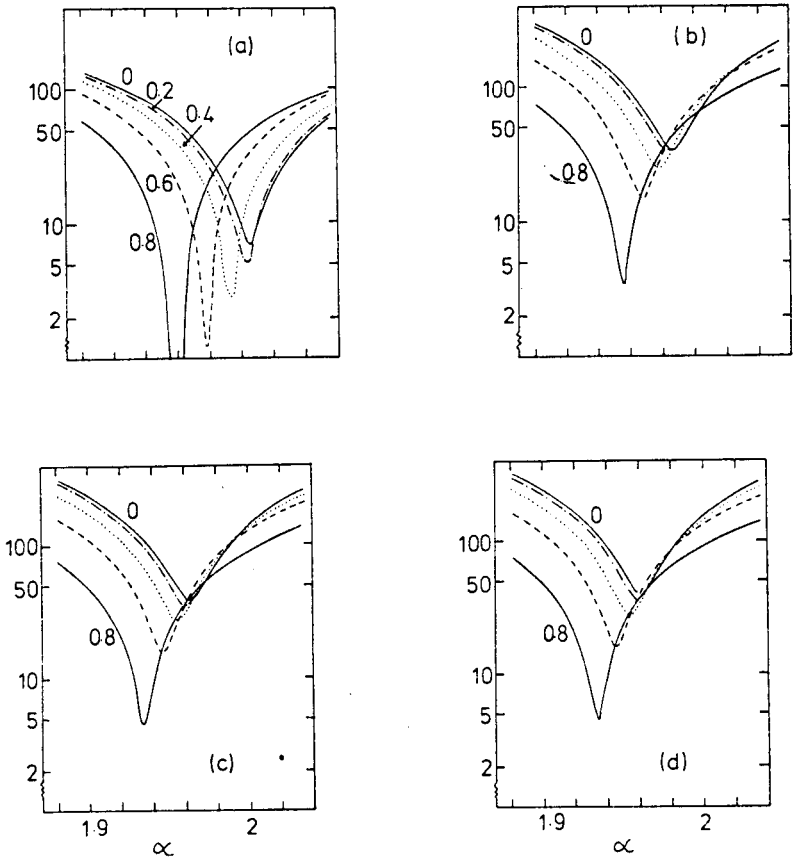

Figure 13 R.M.S. pulse width as a function of α for a fibre excited by a Gaussian beam of varying position and angular spread. The normalized source position is indicated on the curve, $\Delta = 0.02$ and γ_G = (a) 10°; (b) 20°; (c) 30° and (d) 40°. The ordinate is $\sigma/\tau_0 \times 10^7$.

which propagate over a longer time interval.* Moreover, because the range of β_n values excited by sources at different points are quite distinct (see Fig. 12a), the resulting output pulse shapes are also easily distinguished. As the beam spread increases, the curves merge because: (a) for any one source point the transmitted power is more equally distributed among the modes excited and (b) the spectra of modes excited by the various source points increasingly overlap.

The set of curves in Fig. 13 shows the variation of r.m.s. pulse width with α, the source position and its angular spread. The times involved are clearly at least an order of magnitude smaller than those obtained with any of the other sources investigated here and, in the case of the narrowest beam, even smaller still. However, in this last case, the assumption of a point source becomes somewhat suspect so that the result must be treated with some caution.

*Such double-peaked pulses have recently been observed by Cohen [9] and Ikeda and Yoshikiyo [10]. The latter attribute the second peak to irregularities in the refractive index profile but our analysis shows that such a peak can arise even when the profile is perfectly smooth.

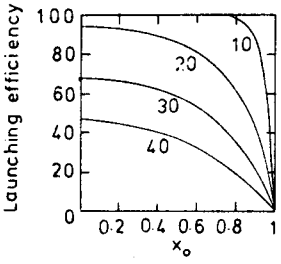

Figure 14 Launching efficiency as a function of source position for a fibre excited by Gaussian beams of the indicated angular spread. The curves are calculated for the fibre $\Delta = 0.02$ and $\alpha = 2$ but there is *very* little variation with α in the range considered in this paper.

Furthermore, just as in the plane-wave case, we must balance against these short pulse widths the decreasing launching efficiency as the spot moves away from the centre of the fibre (see Fig. 14). However, an optimum launching position and spot size can be determined for a given α-profile, once a minimum launching efficiency is specified.

4. Conclusions

Using the WKB approximation to relate group delay to mode parameters (and with a minimum of computing) we have studied the effect of changes in source distribution on the mode launching and impulse response of graded index optical fibres with refractive index profile described by an α-law. We have found that considerable variation in the pulse dispersion can arise from factors such as the focussing of the source and its alignment. More specifically,

(i) Fig. 2 shows that focussing an LED (which we have represented by the truncation of a Lambertian source) increases the r.m.s. pulse width;

(ii) Fig. 5 shows that while increasing the launching angle of an unfocussed laser (plane wave) source decreases the r.m.s. pulse width, for $\alpha \lesssim 2 - \Delta$, the Lambertian source actually leads to shorter pulse times; and

(iii) according to Figs. 13a–d a substantial improvement in pulse dispersion can be obtained by using a focussed laser source incident near the core periphery. The reduced pulse width must be weighed against a corresponding reduction in launching efficiency but for a specific α-profile and launching efficiency requirement, the optimal beam waist and launching position can be found from these results.

The response to these basic sources can also be used to deduce the response to more complex launching conditions by appropriate superposition of plane waves or Gaussian beams.

While the results predicted are confined to α-profiles, the general result given by Equation 16 is not similarly restricted; nor is the exclusion of material dispersion necessary, provided one can write down an expression for group delay in terms of the mode propagation constant, which is independent of the azimuthal mode number, ν (using Arnaud's [4] dispersion factor, for example). However, this approach loses its advantage of reducing numerical computations if the ν-integration in Equation 12 cannot be performed analytically. Under such circumstances, a general numerical technique such as that of Arnaud and Fleming [7] would seem to be the most useful.

Appendix

Either WKB or ray analyses lead to an integral expression for group delay:

$$\frac{\tau_g}{\tau_0} = \frac{\int_{x_i}^{x_0} g(x)[g(x) - \beta_n^2 - l^2/x^2]^{-1/2}\,\mathrm{d}x}{\int_{x_i}^{x_0} \beta_n[g(x) - \beta_n^2 - l^2/x^2]^{-1/2}\,\mathrm{d}x}$$

where x_0 and x_i are the zeros of the denominator in the integrand and $l = \nu/ak_0$.

For an α-profile,

$$\frac{\tau_g}{\tau_0} = \frac{1}{\beta_n I}\int_{u_1}^{u_2}(1-2\Delta u^{\alpha/2})[(1-\beta_n^2)u - 2\Delta u^{(\alpha/2)+1} - l^2]^{-1/2}\,du$$

where $u = x^2$ and

$$I = \int_{u_1}^{u_2}[(1-\beta_n^2)u - 2\Delta u^{(\alpha/2)+1} - l^2]^{-1/2}\,du.$$

Using the fact that

$$\frac{d}{du}[(1-\beta_n^2)u - 2\Delta u^{(\alpha/2)+1} - l^2]^{1/2} = \frac{1}{2}[(1-\beta_n^2) - (\alpha+2)\Delta u^{\alpha/2}][(1-\beta_n^2)u - 2\Delta u^{(\alpha/2)+1} - l^2]^{-1/2},$$

we then have

$$\frac{\tau_g}{\tau_0} = \frac{1}{\beta_n I}\left\{\frac{2}{\alpha+2}[(1-\beta_n^2)u - 2\Delta u^{\alpha/2+1} - l^2]_{u=u_1}^{u_2} + \frac{\alpha+2\beta_n^2}{\alpha+2}I\right\}$$

$$= \frac{\alpha+2\beta_n^2}{(\alpha+2)\beta_n},$$

since the first term in brackets is zero at the limits u_1 and u_2.

Acknowledgements

I am very grateful to Dr M. J. Adams for suggesting the problem and for his help and encouragement during the course of this work. I would also like to thank D. N. Payne for his helpful suggestions and the Commonwealth Scientific and Industrial Research Organization of Australia for their financial support.

References

1. W. A. GAMBLING, D. N. PAYNE, C. R. HAMMOND and S. R. NORMAN, *Proc. IEE* **123** (1976) 570–6.
2. W. G. FRENCH, G. W. TASKER and J. R. SIMPSON, *Appl. Opt.* **15** (1976) 1803–7.
3. R. OLSHANSKY, *ibid* **14** (1975) 935–45.
4. J. A. ARNAUD, *Bell Syst. Tech. J.* **54** (1975) 1179–205.
5. C. C. TIMMERMANN, *A.E.U.* **28** (1974) 144–5.
6. R. OLSHANSKY and D. B. KECK, *Appl. Opt.* **15** (1976) 483–91.
7. J. A. ARNAUD and J. W. FLEMING, *Elect. Lett.* **12** (1976) 167–9.
8. R. OLSHANSKY, *Appl. Opt.* **15** (1976) 782–8.
9. L. G. COHEN, *ibid* **15** (1976) 1808–14.
10. M. IKEDA and H. YOSHIKIYO, *ibid* **15** (1976) 1307–12.
11. C. C. TIMMERMANN, *A.E.U.* **28** (1974) 186–8.
12. C. C. TIMMERMANN and K. PETERMANN, *ibid* **29** (1975) 235–7.
13. D. B. KECK, *Appl. Opt.* **13** (1974) 1882–8.
14. J. P. HAZAN, L. JACOMME and D. ROSSIER, *Opt. Commun.* **14** (1975) 368–73.
15. L. JACOMME, *Appl. Opt.* **14** (1975) 2578–84.
16. D. GLOGE and E. A. J. MARCATILI, *Bell Syst. Tech. J.* **52** (1973) 1563–77.
17. M. J. ADAMS, D. N. PAYNE and F. M. E. SLADEN, *Elect. Lett.* **11** (1975) 238–40.
18. S. D. PERSONICK, *Bell Syst. Tech. J.* **52** (1973) 1175–94.
19. J. P. DAKIN, W. A. GAMBLING, H. MATSUMURA, D. N. PAYNE and H. R. D. SUNAK, *Opt. Commun.* **7** (1973) 1–5.
20. M. EVE, *Opt. Quant. Elect.* **8** (1976) 285–93.
21. A. W. SNYDER and C. PASK, *J. Opt. Soc. Am.* **63** (1973) 806–12.
22. D. MARCUSE, *Bell Syst. Tech. J.* **54** (1975) 1507–30.